

Red galaxies with pseudo-bulges in the SDSS: closer to disk galaxies or to classical bulges?

B. Ribeiro^{1*} and C. Lobo^{2,3} and S. Antón^{4,5} and J.M. Gomes³ and P. Papaderos³

¹ Aix Marseille Université, CNRS, LAM (Laboratoire d'Astrophysique de Marseille) UMR 7326, 13388, Marseille, France

² Departamento de Física e Astronomia, Faculdade de Ciências, Universidade do Porto, Rua do Campo Alegre 687, PT4169-007 Porto, Portugal

³ Instituto de Astrofísica e Ciências do Espaço, Universidade do Porto, CAUP, Rua das Estrelas, PT4150-762 Porto, Portugal

⁴ Instituto de Astrofísica de Andalucía (CSIC), Glorieta de la Astronomía, s/n 18008, Granada, Spain

⁵ Instituto de Astrofísica e Ciências do Espaço, Universidade de Lisboa, Faculdade de Ciências, Campo Grande, PT1749-016 Lisboa, Portugal

ABSTRACT

Pseudo-bulges are expected to markedly differ from classical, quasi-monolithically forming bulges in their star formation history (SFH) and chemical abundance patterns. To test this simple expectation, we carry out a comparative structural and spectral synthesis analysis of 106 red, massive galaxies issued from the SDSS, subdivided into bulgeless, pseudo-bulge and classical bulge galaxies according to their photometric characteristics, and further obeying a specific selection to minimize uncertainties in the analysis and ensure an unbiased derivation and comparison of SFHs. Our 2D photometry analysis suggests that disks underlying pseudo-bulges typically have larger exponential scale lengths than bulgeless galaxies, despite similar integral disk luminosities. Spectral synthesis models of the stellar emission within the 3'' SDSS fiber aperture reveal a clear segregation of bulgeless and pseudo-bulge galaxies from classical bulges on the luminosity-weighted planes of age-metallicity and mass-metallicity, though a large dispersion is observed within the two former classes. The secular growth of pseudo-bulges is also reflected upon their cumulative stellar mass as a function of time, which is shallower than that for classical bulges. Such results suggest that the centers of bulgeless and pseudo-bulge galaxies substantially differ from those of bulgy galaxies with respect to their SFH and chemical enrichment history, which likely points to different formation/assembly mechanisms.

Key words: galaxies: bulges – Galaxies: evolution – galaxies: general – Galaxies: stellar content

1 INTRODUCTION

The study of galaxy bulges has gained significant momentum lately, much due to the realization that the nature and formation history of these structural components of galaxies is far more intricate and diverse than what was considered to be some years ago. It has been suggested that some bulges - named pseudo-bulges - emerged through a prolonged star-formation process that is fed through disk material in the course of the secular galaxy evolution, in contrast to classical bulges, which are thought to assemble through quasi-monolithic gas collapse and/or mergers early on (for a review see Kormendy & Kennicutt 2004, see also references therein). Due to their distinct formation history, pseudo-bulges are thus expected to appreciably differ from classical bulges in their stellar content (age, metallicity, dynamics, morphology and structure) and current star formation rate (SFR).

Reproducing the formation of these structures within the hierarchical merging paradigm of galaxy formation and evolution is challenging (see, e.g., Okamoto 2013, and references therein) yet of considerable relevance, as nearby disk galaxies frequently host structures that can be considered as pseudo-bulges (e.g. Kormendy et al. 2010; Simard et al. 2011; Fisher & Drory 2011; Bennert et al. 2014).

Kormendy & Kennicutt (2004) list several characteristics that can be used to identify pseudo-bulges, one of them being a surface brightness profile (SBP) that is shallower than the one displayed by classical bulges. A fit with a Sérsic law to pseudo-bulges is thus expected to yield a lower Sérsic index η (generally <2 , i.e. closer to the value ≈ 1 that is typical for disks) instead of the high η (3–6) that is characteristic of massive galaxy spheroids, and closer to the de Vaucouleurs law. A significant degree of rotational support and diskiness are regarded as further signatures of pseudo-bulges. Their distinctiveness in terms of structural, morphological and kinematic properties, relatively to what

* E-mail: bruno.ribeiro@lam.fr

one historically calls a bulge, is now relatively well established and widely used to identify them (e.g. Fisher & Drory 2008; Gadotti 2009).

Finer photometric details, harder to observe and hardly hinted on SBPs, may further help identifying pseudo-bulges. Unsharp masking techniques applied to images often reveal underlying structural features (spiral arms, bars, rings, small scale disks) considered to be typical of pseudo-bulges (e.g., Kormendy & Kennicutt 2004 and references therein). These sometimes co-exist with a classical bulge (see e.g. Erwin et al. 2015) and are thought to be built up from the disk material, also based on kinematics (see also e.g. Kehrigh 2012 for detection of such structures in early-type galaxies possessing a warm inter-stellar medium). This lends further support to a “gentler” formation mechanism that is associated with internal gravitational disk instabilities and prolonged star-forming activity that could be sustained by gas accretion from the galaxy environment, rather than quick growth through merging and the ensuing violent relaxation of the stellar component. Mergers were - at least until recently - commonly expected to destroy disks in general, and likely also the faint spiral signatures described above, rather giving rise to a classical bulge (eg Naab & Trujillo 2006; Hopkins et al. 2010). Nevertheless, there is also some theoretical and observational evidence for the survival of disks after mergers, or the existence of pseudo-bulge structures in merger remnants (Keselman & Nusser 2012; Ueda et al. 2014; Querejeta et al. 2014, and references therein). Alternatively, Guedes et al. (2013) propose a scenario where mergers possibly induce rapid growth of pseudo-bulges out of disk material in the early stages of galaxy assembly. In this scenario the structure that we recognize as a pseudo-bulge today results from the complex evolution of a stellar bar that suffers repeated stages of formation and dissolution along the galaxy’s evolution. Indeed, bars are thought to drive physical processes that lead to pseudo-bulge formation (Combes et al. 1990; Kormendy & Kennicutt 2004; Kubryk et al. 2013; see also Mendez-Abreu et al. 2014 and references therein) traditionally in a secular way. But other authors minimize the contribution provided by secular bar instabilities to the assembly of pseudo-bulges in favour of physical mechanisms occurring at much smaller timescales like e.g. high-redshift starbursts (Okamoto 2013) or minor mergers (Eliche-Moral et al. 2011).

Given the plethora of possibilities, the existence of specific structural components such as embedded bars should not, in principle, be a requirement for identifying a pseudo-bulge. And, somewhat in tandem, the timescale for the formation of the pseudo-bulge (thus the dominant mechanism leading to its formation, provided that there is a unique one) is not yet pinned down either; neither by simulations nor even by observations. Still on the latter, a recent analysis based on the colors of a sample of isolated galaxies seems to discard as well the need for long timescales for the formation of pseudo-bulges: Fernández Lorenzo (2014) finds that the majority of their pseudo-bulges show colors compatible with the red sequence of early-type galaxies, thus advocating “an early formation epoch and not much subsequent growth”. However, the family of pseudo-bulges might be far more diverse, with the old entities described (Fernández Lorenzo 2014) constituting merely a sub-branch of it. In fact, several previous studies document the presence

of younger, bluer stellar populations and significant SFR in pseudo-bulges (e.g., Morelli et al. 2008; Fisher et al. 2009; Gadotti 2009; Zhao 2012 and references therein), consistent with a time-continued build-up process, in contrast to that undergone by classical bulges.

All these works show that the defining characteristics - in particular in what concerns stellar populations and morphological substructure - and origin of pseudo-bulges are far from being well understood. A thorough census and analysis of pseudo-bulges is thus imperative to allow for advances to be made in this field. And, starting by the nearby systems, which can be more easily observed, is an obvious choice.

The aim of this study is to contribute to our understanding of such structural entities, using a sample of galaxies selected on stringent criteria, and employing a stellar population synthesis (SPS) approach, which has not yet been very much explored and can provide relevant constraints. Indeed, stellar ages, metallicities, star formation histories (SFHs) and other parameters inferred from SPS can give insight into the formation mechanism of pseudo-bulges and help addressing whether it is distinct from that of classical ones. Our sample comprises galaxies with little or absent ongoing star formation, mainly to avoid the difficulties in the analyses of their SBPs that are due to light contamination by HII regions and associated features (e.g., nebular emission, dust lanes), that complicate the determination of the Sérsic index η in SBP fitting. This selection is described in Sect. 2, where we also detail the criteria adopted to divide the sample into different structural classes and identify pseudo-bulge hosts. With this deliberate bias in star-forming activity (and color), the SPS should also be more reliable (due to faint emission lines and insignificant continuum nebular emission). We thus expect that, if any difference in the SFHs and stellar metallicities between pseudo-bulges and classical ones is still uncovered, then this should provide a robust indication. In Section 3 we give a brief explanation of the method used to infer the main physical properties of the analyzed pseudo-bulges through spectral modeling of their SDSS spectra. In Section 4 we provide and discuss the main results from our analysis. Finally, in Section 5 we summarize the main points to be taken from this work.

Throughout the paper we use WMAP7 cosmology: $H_0=71 \text{ km s}^{-1} \text{ Mpc}^{-1}$, $\Omega_m=0.27$ and $\Omega_\Lambda=0.73$ (Larson 2011).

2 THE SAMPLE - SELECTION CRITERIA AND DEFINITION OF STRUCTURAL CLASSES

This study is largely motivated by and builds upon our previous work in Coelho et al. (2013) that focused on a sample of massive red galaxies selected from the same NYU-VAGC catalogue of Blanton et al. (2005) to ascertain the frequency of active galactic nuclei (AGN) hosted by quiescent galaxies with a negligible or absent bulge. Since the Coelho et al. (2013) sample was restricted to low Sérsic indices ($\eta < 1.5$), we have extended it to include as well galaxies where the bulge has a significant contribution to the total light of the galaxy. We thus select SDSS DR7 galaxies from the same NYU-VAGC catalogue of Blanton et al. (2005) that gathers

photometric and structural parameters for all SDSS galaxies having spectroscopic data. All objects obey the following requirements:

- redshift in the range $0.02 < z < 0.06$;
- galaxy stellar mass $M_* > 10^{10} M_\odot$, computed as in Bell (2008) from the r-band SDSS luminosity and g-r color, and assuming a Chabrier (2003) initial mass function;
- color index $(g - r)$ typical of red galaxies: $(g - r) > 0.57 + 0.0575 \log(M_*/10^8 M_\odot)$ (Bell 2008);
- inclination cut equivalent to $i \lesssim 60^\circ$ to exclude edge-on systems, prone to biases in the photometric and SPS analysis due to dust extinction (see Coelho et al. 2013).

These criteria yield a sample of galaxies with expected little star formation activity. On top of the above, we also carried out a visual inspection of the SDSS multi-wavelength images to discard galaxies with features obviously related to star formation, close-by or overlapping objects, as well as galaxies with interaction-induced distortions and complex morphologies (i.e., star-forming rings, tails and bridges, prominent dust lanes), since all these could compromise a robust estimate of the galaxies' structural properties, in particular in what regards the bulge. This second selection stage was also meant to minimize the number of obscured objects, which indeed was found to be the case in the subsequent analysis (Sect. 4.4).

We expect this strategy to greatly simplify the morphological analysis and render it more robust, while introducing no bias in what concerns the main objective of this work: to investigate a possible significant difference in the stellar ages, metallicities and other properties of pseudo-bulges when compared with classical bulges. More specifically, our main goal is to explore trends with regard to the above quantities or plainly to verify whether there are obvious contradictions to a scenario of different formation mechanisms/timescales between bulges and pseudo-bulges.

The adopted redshift interval and mass cutoff aim at obtaining a compromise of having enough objects in the sample, a good spatial coverage in photometry (for inspecting galaxy images and deriving significant SBPs), adequate spectroscopic sampling of their central regions and no particular correlations of the derived parameters with galaxy mass (due to the exclusion of low-mass objects).

The above selection criteria imposed a limit on massive, almost face-on, pure disks with red colors of about 35 (for the redshift range in question). The advantage of having a relatively small sample¹ is that its size allows doing a dedicated analysis of each object. The approximately same number of galaxies was sought (in the same volume) to populate the other classes, resulting in a total of 106 objects. Their morphological classification is discussed in the next sub-section.

¹ Because red late-type galaxies are rare (e.g., Bamford et al. 2009; Masters et al. 2010; Coelho et al. 2013), a consequence of adopting our color selection is to drastically reduce the number of objects of later types, so our aim cannot possibly be to compile large samples that offer statistical robustness to the results.

2.1 Structural analysis of the sample

One of the commonly used ways to distinguish between bulge dominated galaxies and disk dominated ones, and assess the significance of the bulge when it is present, is to fit a Sérsic (1968) profile

$$\Sigma(r) = \Sigma_e \exp[-\kappa(r/r_e)^{1/\eta} - 1] \quad (1)$$

where the index η describes the shape of the SBP, r_e is the effective radius, Σ_e is the surface brightness at radius r_e and κ is a parameter coupled to η (Ciotti & Bertin 1999), such as to ensure that half of the total flux is enclosed within r_e . A Sérsic index of $\eta = 1$ corresponds to a pure exponential profile that is typical for galactic disks, whereas $\eta = 4$ corresponds to the de Vaucouleurs profile associated to elliptical galaxies and low-mass galaxy spheroids.

Though values of η were already available for our galaxies in the NYU-VAGC catalog, these were obtained through the fitting of equation 1 to the azimuthally averaged radial profile of each galaxy, convolved with the estimated seeing (Blanton et al. 2005). By definition, such a profile determination and fitting technique collapses a 2D image into a 1D SBP. Although this transformation is straightforward in its practical application, and permits a standardized quantification of galaxy structural properties, it obviously entails loss of information. For example, one can infer from decomposition of an SBP the total magnitude and mean isophotal radius of a structural component (e.g., a bar) but important morphological properties (e.g., position angle, ellipticity and boxiness/diskiness) are irretrievable from a 1D SBP. 2D surface photometry techniques, now commonly used, can, in principle, preserve much of the 2D information in a galaxy image, and it has been claimed on the basis of simulations that they can better recover galaxy structural components, when these follow simple empirical laws (Wadadekar et al. 1999; Guo et al. 2009).

We performed 2D photometry modeling with GALFIT² (Peng et al. 2002, 2010, version 3.0) to the r-band SDSS images, with the goal of analysing in more detail the structural parameters of the selected galaxies and assigning them to different morphological subsamples. To each of the 106 galaxies we carried out a fit with a single Sérsic (equation 1) to the entire galaxy. Two types of galaxies (60% of the whole sample) were well fit using this strategy: those described by a Sérsic law with $\eta = 1$ (38 galaxies, hereafter named disks or bulgeless galaxies) and another group well modeled by a Sérsic function with $\eta > 3$ (26 galaxies, for which no disk component was required - what we will call the bulgy galaxies). However, results were inadequate for the remaining 40% of the sample (42 galaxies) since we identified significant signal in the residuals image. The SBP of these objects was thus refit with a multi-component model consisting of an exponential disk plus a Sérsic profile - translated by the following equation:

$$\Sigma(r) = \Sigma_{e,d} \exp[-\kappa(r/r_{e,d}) - 1] + \Sigma_{e,b} \exp[-\kappa(r/r_{e,b})^{1/\eta_b} - 1]. \quad (2)$$

where subscripts d and b refer to disk and bulge components, respectively. This allowed to obtain good results for the whole sample (residuals after model subtraction amount

² <http://users.obs.carnegiescience.edu/peng/work/galfit/galfit.html>

to less than 10% of the galaxy flux). No additional constraint on the profiles, aside from the fixed Sérsic index for the disk component (when required) in equation 2, was imposed on all fits. The sky component was fitted locally and simultaneously using an image with a constant value close to that reported from the SDSS. The errors associated with each pixel are computed internally by GALFIT from a combination of the rms of the sky regions and the pixel signal assuming a poissonian distribution of the noise³.

Consistency tests led us to confirm the goodness of this strategy where we fit a fixed $\eta = 1$ Sérsic law plus a free- η Sérsic profile (i.e., equation 2) to all galaxies⁴ since it turned out to be more robust against possible variations in the other structural parameters, and to yield more physically meaningful results. Additionally, fitting a pure exponential disk to the extended regions of the galaxy allows for a consistent measurement of the light in excess to it, which can plausibly be attributed to the bulge emission. This more robust approach is also justified by an important goal of this study, namely to quantify the significance and luminosity contribution of the bulge even for almost bulgeless objects showing a merely minor luminosity surface brightness enhancement at the centers of their disk though having no conspicuous sub-structure (like bars, rings, etc).

The final step of this stage was to identify pseudo-bulges among the group of 42 galaxies that revealed an SBP where two structural components were obvious and compelling (a disk plus a bulge with Sérsic index η_b assuming various values). To do so, a frontier value for η_b was sought. In general terms, and since η varies continuously from a Gaussian profile (0.5) through an exponential disk (1.0) and to a classical bulge (~ 4), it is not easy to objectively establish a boundary value separating bulgy galaxies from those hosting a pseudo-bulge, or bulgeless ones. After a careful visual inspection of the images and the results from GALFIT, and by considering previous studies (Bell 2008; Gadotti 2009; Barentine & Kormendy 2012), we finally adopted the conservative range of $\eta_b < 1.5$ to identify pseudo-bulges - these total 29 in our sample. The remaining 13 galaxies will be henceforth referred to as intermediate- η bulge galaxies. To summarize this procedure and the adopted classes, we present in table 1 the selection criteria applied to SBPs and the final number of galaxies in each class for our 106 objects. Typical examples of galaxies of each class may be found in figure 2, and respective redshift distributions are given in figure 1. This figure also shows that there is no trend on the frequency of bulge type with redshift, so we expect that any change there may be on the physical resolution of SDSS images along the redshift interval probed by our sample will have no major impact on the fits to the galaxies SBPs. The reader is referred to Coelho et al. (2013) for more details on the fitting procedure and construction of the 1D surface brightness profiles shown in figure 2 for illustration purposes.

A concluding verification was carried out on the performance of GALFIT as compared to the specific adaptation

³ For a detailed description on how this is done please refer to <http://users.obs.carnegiescience.edu/peng/work/galfit/CHI2.html>

⁴ Note that, in practice, equation 2 was fit to all galaxies, considering that the second term is null in the case of bulgeless galaxies whereas it's the first term that is canceled for pure spheroids.

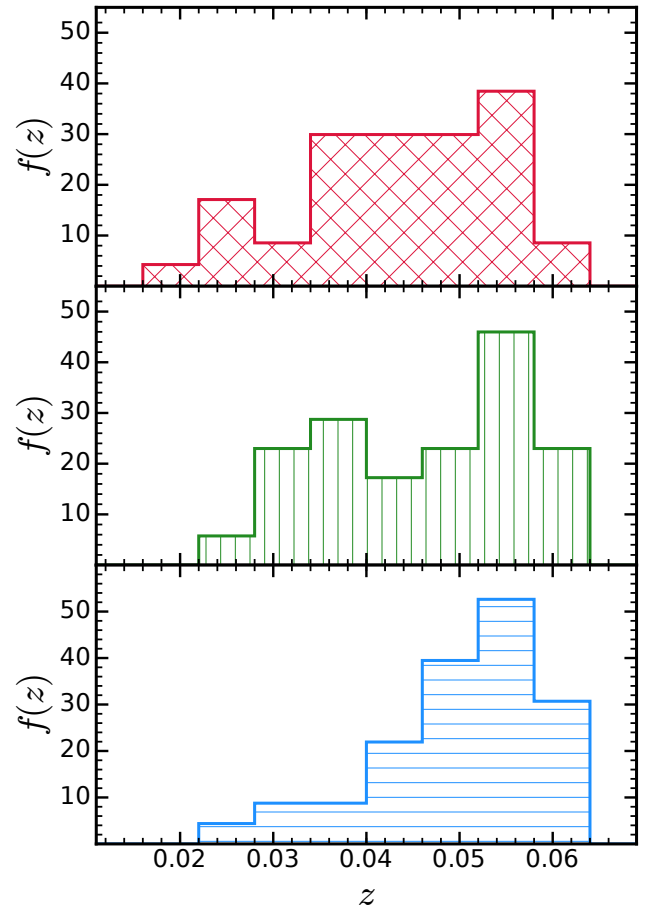


Figure 1. Redshift distribution of the different sub-samples. Top: intermediate+bulgy (these two classes are merged for the purpose of SPS studies, as detailed in section 4.2); Middle: pseudo-bulge; Bottom: bulgeless. $f(z)$ represents the number of galaxies divided by the integral of the distribution, for normalization.

of 1D surface photometry by Blanton et al. (2005). After defining our classes, we fitted the SBPs of our bulgeless and pseudo-bulge galaxies with a single Sérsic model (equation 1), and compared our values for η with those reported in the NYU-VAGC catalog for the same r-band images. Fig. 3 reports the results, where we find that our 2D analysis yields a better separation between bulgeless and pseudo-bulge galaxies. An additional reason for this may also lie in the automatized treatment of the whole SDSS dataset by Blanton et al. (2005), that obviously cannot handle the particularities of individual galaxies, which is perfectly acceptable in million-object catalogs used for large statistical studies.

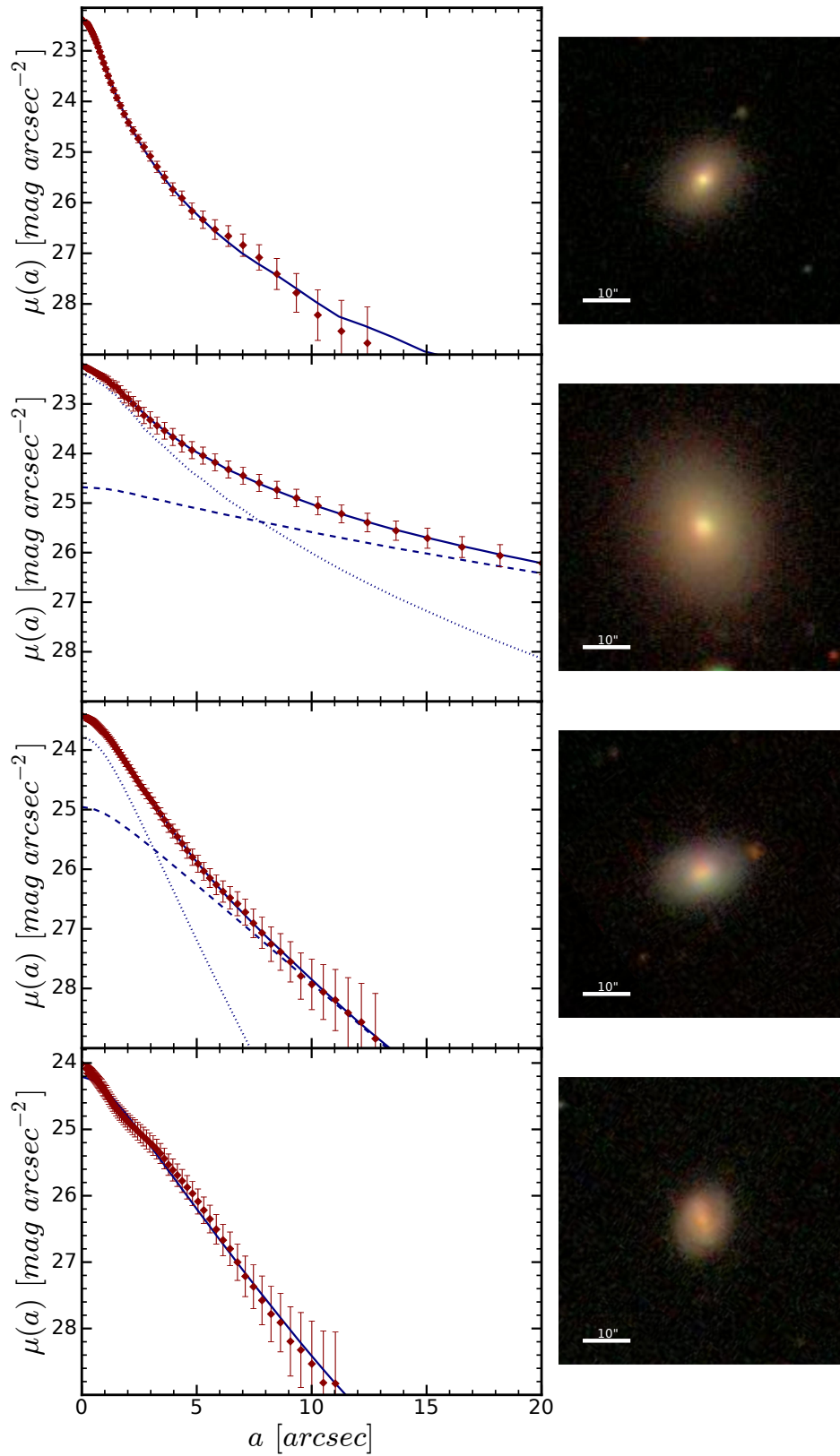


Figure 2. Left: typical examples of 1D surface brightness profiles (SBP) for each of the 4 classes, from top to bottom: bulgy, intermediate- η , pseudo-bulge, bulgeless. The solid lines correspond to the SBP of the global model, dashed lines correspond to the disk component and dotted lines to the bulge component. Right: SDSS *gri* color-composite cutout image of each source considered. Image size is fixed (to $\sim 60''$ in side).

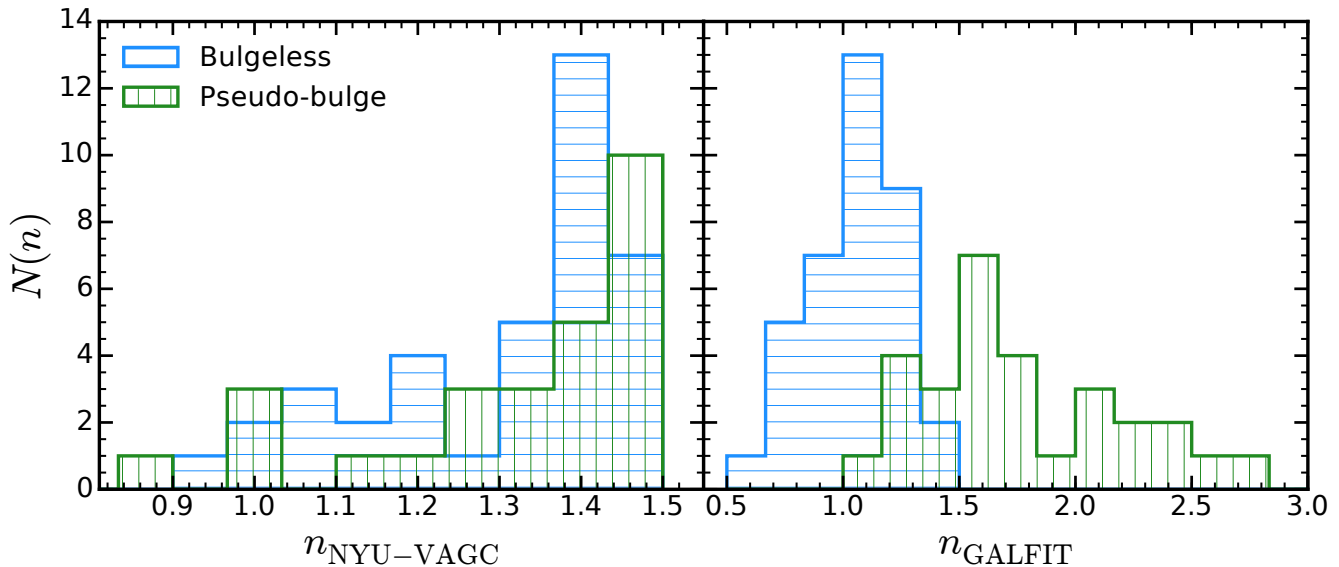


Figure 3. Results of the test comparing the η values issued from fitting a single Sérsic model in 2D (with GALFIT; on the right) and in 1D (by Blanton et al. 2005 - values available in the NYU-VAGC catalog; on the left). The galaxies used for this test are the ones we classified (by a different procedure - see text and equation 2) as bulgeless (in blue) and pseudo-bulge galaxies (in green).

Table 1. Structural classes of galaxies considered, definition of each class based on the exponent η of the best-fitting 2D Sérsic model and number of objects in each class. Profile decomposition was made using a combination of two Sérsic laws (see equation 2): one with fixed $\eta_d = 1$ (to model the disk) and another one with the Sérsic index η_b let free when fitting the bulge component. Pure-disk galaxies obviously do not require an additional Sérsic component whereas bulgy galaxies were fitted by a single Sérsic model, without need for an additional underlying disk.

Structural class	interval of Sérsic index for objects in this class	number of galaxies
bulgeless galaxies	$\eta_d = 1$, no bulge component	38
pseudo-bulge galaxies	$\eta_d = 1$, $\eta_b < 1.5$	29
intermediate- η bulge galaxies	$\eta_d = 1$, $1.5 < \eta_b < 3.5$	13
bulgy galaxies	$\eta_b > 3$, no disk component	26

3 SPECTRAL SYNTHESIS OF STELLAR POPULATIONS

The analysis of the SDSS spectra of our 106 galaxies of different structural classes was undertaken using the stellar population synthesis code STARLIGHT⁵ (Cid Fernandes et al. 2005) to model the spectral energy distribution (SED) of galaxies with a linear superposition of N_* Simple Stellar Populations (SSPs). The best-fitting solution from STARLIGHT is obtained via standard χ^2 minimization with a non-uniform sampling of the parameter space. This code employs advanced statistical mechanics techniques, such as simulated annealing and multiple independent Markov Monte Carlo Chains to avoid convergence into local minima. Additionally, the Gelman & Rubin (1992) convergence criterion is implemented for a better determination of the global minimum solution.

The star formation and chemical enrichment history of a galaxy is obtained from the best-fitting light population vector $\vec{x} = (x_1, \dots, x_{N_*})$, i.e. the set of fractional contributions of stellar populations with different ages and metallicities. The mass population vector $\vec{\mu}$ is derived indirectly,

after combining \vec{x} with the corresponding SSP mass-to-light ratios (M_*/L). In order to have a more realistic modeling, extinction and kinematic parameters are also taken into account. For the former a uniform dust screen and the Cardelli et al. (1989) reddening law were adopted and for the latter we use a Gaussian kernel $G(v_*, \sigma_*)$ that is determined by two parameters: the systemic velocity v_* and the velocity dispersion σ_* that model the line shifts and broadening effects, respectively.

Besides the main products issued from the STARLIGHT fits, we can also use these fits to accurately extract and measure any remaining emission-lines. For this, we have subtracted the best-fitting stellar SED from the observed spectrum in order to isolate the pure emission-line spectrum. This procedure is crucial, especially for bulgy galaxies that usually exhibit very weak emission-lines, but also possibly for several of the remaining objects (due to our selection described in section 2).

3.1 Inferred physical properties from multiple STARLIGHT fits

In our analysis, we make use of the evolutionary synthesis models from Bruzual & Charlot (2003) to compute a set of

⁵ <http://www.starlight.ufsc.br/>

150 SSPs that comprise 25 ages (from 1 Myr to 15 Gyr, covering all evolutionary phases of single bursts) for 6 metallicities: 1/200, 1/50, 1/5, 2/5, 1, 2.5 Z_{\odot} , where the solar value Z_{\odot} is 0.02. These models are based on the ‘‘Padova 1994’’ evolutionary tracks (Alongi et al. 1993; Bressan et al. 1993; Fagotto et al. 1994a,b; Girardi et al. 1996) and the Chabrier (2003) initial mass function between 0.1 and 100 M_{\odot} .

Due to the probabilistic nature of the solutions from STARLIGHT, the population vector obtained for a spectrum can slightly vary among different fits. In order to estimate the impact of this inherent dispersion in model fits on the spectral synthesis parameters, we have devised a new approach where 50 STARLIGHT runs were done for each galaxy spectrum to better quantify systematic uncertainties in the mean stellar age and metallicity, stellar mass and velocity dispersion, among other spectral synthesis quantities, and also to have a better error statistics on the emission-lines and line ratios measured after the removal of the underlying stellar contribution.

We note that all results obtained with STARLIGHT apply to the SDSS fiber spectra (aperture 3’), which enclose only the central parts of galaxies, so the spectral synthesis parameters refer to a projected area with a diameter between ~ 1.2 and ~ 3.4 kpc for the most nearby and most distant sources in our galaxy sample, respectively.

4 PSEUDO-BULGE GALAXIES IN OUR SAMPLE - SIMILAR TO DISKS OR RATHER TO CLASSICAL BULGES?

In order to gain insight into the nature and most likely origin of pseudo-bulges we compared several parameters obtained both from the structural analysis and stellar population synthesis, previously described in sections 2.1 and 3, respectively. As stated before, the aim is to verify whether there is evidence for distinguishing pseudo-bulges from classical bulges, and lending support to a disparate nature and evolutionary scenario between both.

4.1 Structural parameters

Table 2 and figures 4 and 5 summarize the trends that our analysis of the structural parameters reveal.

Although the dispersion of values is somewhat large, along the sequence bulgeless \rightarrow pseudo-bulge \rightarrow intermediate- η bulge galaxies, there is a monotonous increase of the effective radius of the disk component, $r_{e,d}$ (≈ 1.7 exponential scale lengths), for galaxies with similar absolute disk magnitudes in the r band. This is apparent from the histogram in Fig. 4, as well as in the median value (Table 2; mean values reflecting the same trend). A similar though less pronounced behavior was obtained by Gadotti (2009) for a sample of nearly 1000 SDSS galaxies selected and analysed in a different way.

As for absolute magnitudes (Fig. 5 and Table 2), while disks and pseudo-bulge galaxies span quite the same range of both total and disk luminosities, intermediate- η bulge galaxies tend to have slightly brighter disks on average. The two classes hosting classical bulges (bulgy and intermediate- η) reach up to brighter absolute total magnitudes, likely due to the relevant bulge contribution.

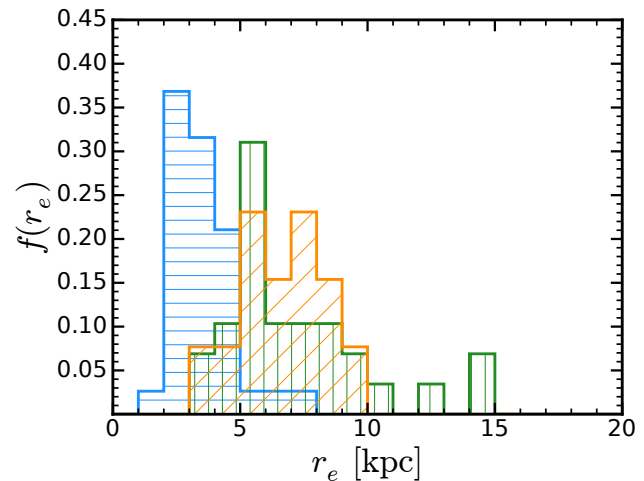


Figure 4. Normalized histograms of the values of the disk effective radius, $r_{e,d}$, for the three classes having a disk component: blue is for pure disks, green refers to pseudo-bulge galaxies, while the orange histogram shows values for the intermediate- η bulge galaxies.

By comparing galaxies having a disk component in their SBP (i.e. a non-null first term in equation 2), the trends shown in this section suggest that the exponential disks of pseudo-bulge galaxies are more diffuse (larger values for $r_{e,d}$) than those of bulgeless galaxies, since they share quite comparable absolute magnitudes. One should bear in mind though that this might be partly due to the addition of a second component to the fit for the first class of galaxies: the Sérsic function that models the bulge component (mainly the central light excess), leaves the pure exponential to model best the outer, fainter regions of the galaxy to a larger extent when compared to the single disk fit applied to bulgeless galaxies. Despite the fact that this may artificially increase the size of the disk by the simple additional presence of a central component, the difference in sizes observed in Figure 4 cannot be attributed to the fitting procedure. This was tested by applying the 2-component fit (equation 2) to bulgeless galaxies - in these conditions, the effective radii of their disk component remained systematically smaller than for pseudo-bulge galaxies, fitted in exactly the same way.

Behind the trends observed in Figure 5 (left panel) is likely a well known correlation: classical bulges are usually found in galaxies more massive (and thus brighter) than those hosting pseudo-bulges and these, in turn, are more massive (and brighter) than pure disk galaxies (e.g. Fisher & Drory 2011). We verify this trend in our sample since the estimate we perform - through equation (1) of Bell (2008) - gives mean values of 10.2, 10.3 and 10.5 for the logarithm of the total stellar mass of, respectively, disk galaxies, galaxies hosting pseudo-bulges and the remaining galaxies (hosting classical bulges). A wider discussion on the impact of the mass of galaxies on the properties of bulges is, however, beyond the scope of this paper.

4.2 Stellar population synthesis parameters

Typical spectra of objects assigned to our structural classes are shown in figure 6. Different spectrophotometric charac-

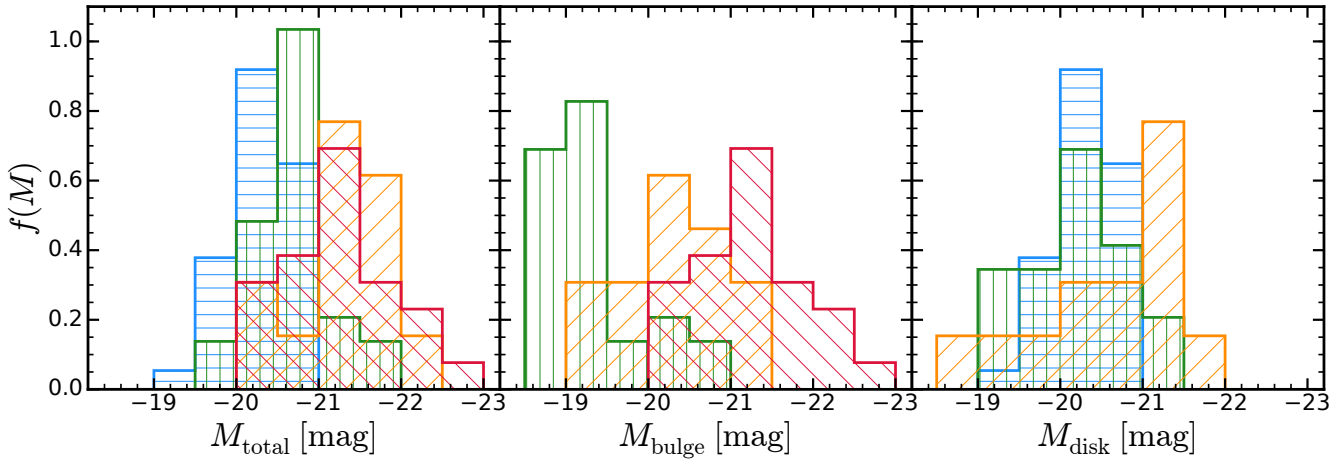


Figure 5. Normalized histograms of the total (left panel), bulge (middle panel) and disk (right panel) absolute magnitudes in the r-band for all structural classes: blue is for pure disks, green refers to pseudo-bulge galaxies, the orange histogram shows values for the intermediate- η bulge galaxies and the red is for bulgy galaxies.

Table 2. Median and dispersion (standard deviation) values for some of the parameters inferred from the structural analysis for each class of galaxies (presented in section 2.1): total absolute r-band magnitude ($M_r(\text{total})$), bulge and disk magnitudes ($M_r(\text{bulge})$ and $M_r(\text{disk})$, respectively) and effective radius $r_{e,d}$ of the disk component in kiloparsec.

Structural class	$M_r(\text{total})$	$M_r(\text{bulge})$	$M_r(\text{disk})$	$r_{e,d}$ [kpc]
bulgeless galaxies	-20.3 ± 0.6	–	-20.3 ± 0.6	3.4 ± 1.2
pseudo-bulge galaxies	-20.7 ± 0.5	-19.3 ± 0.6	-20.3 ± 0.6	6.1 ± 2.9
intermediate- η bulge galaxies	-21.3 ± 0.6	-20.2 ± 0.6	-20.7 ± 0.8	6.8 ± 1.6
bulgy galaxies	-21.1 ± 0.6	-21.2 ± 0.6	–	–

teristics are evident: while classical bulges tend to be redder and essentially lack conspicuous emission-lines, pseudo-bulges and the central regions of bulgeless galaxies are bluer and show weak emission-lines, pointing towards recent or ongoing star-formation.

Running STARLIGHT 50 times for each galaxy spectrum allows us to estimate the uncertainties associated with various quantities of interest. We also expect this procedure to offer a more reliable statistical approach, as already stated in section 3. Note that we have considered all SDSS spectra without imposing any restriction in terms of signal-to-noise nor any other quality criterion. In any case, the average S/N in the continuum region (4730–4780 Å) is 22.6 ± 6.9 for the whole sample, the minimum S/N value being 9.3 (for 1 galaxy only), quite sufficient for a good fit.

The population synthesis models yielded very similar trends for bulgy and intermediate- η bulges (i.e. what we have been calling classical bulges or henceforth refer to simply as bulgy galaxies) with a large overlap in what regards many important properties and parameters. For this reason we merged these two classes from here onwards - simply called *bulgy*, standing for bulge dominated galaxies - since they are consistently alike in their stellar populations.

In this section (and in the following one), all plots show both the individual STARLIGHT realizations for each galaxy (as small dots) as well as the corresponding median value (large circles). Bulgy, pseudo-bulge and bulgeless galaxies are distinguishable through colors, being coded as red, green and blue, respectively. A median value of the main param-

eters obtained from STARLIGHT and discussed next are given in Table 3 for each galaxy class, along with the respective 1σ dispersion.

In figure 7 we show two luminosity-weighted quantities: the mean stellar metallicity $\langle Z_* \rangle_L = \sum_{j=1}^{N_*} x_j Z_j$ as a function of the mean stellar age $(\log t_*)_L = \sum_{j=1}^{N_*} x_j \log t_j$, where Z_j and t_j are the metallicity and age of the j^{th} SSP. Despite the spread in the data, especially apparent for later types, we can see a conspicuous increase along the sequence from bulgeless, pseudo-bulges to bulgy galaxies, where the median values for the stellar age were determined to be $1.12 \rightarrow 1.95 \rightarrow 4.79$ Gyr, while the mean stellar metallicity goes from 0.6 to 1.2 Z_\odot . This suggests that centers of bulgeless galaxies and pseudo-bulges span a larger interval on both parameters but, on average, have younger and less metallic stellar populations in comparison with classical bulges. The main reason might be due to the fact that the two former classes are typically more gas-rich and possibly sustain ongoing low-level star formation, whereas almost gas-devoid bulgy galaxies have ceased forming stars early-on after depletion of their gas supply and simultaneous increase of their metal content (see section 4.5).

The mass-metallicity relation for our sample of galaxies is shown in figure 8, where the stellar mass has been corrected for the returned fraction to the inter-stellar medium (ISM) according to Bruzual & Charlot (2003). Although the distributions largely overlap with regard to the total stellar mass enclosed within the fiber, there is a slight increase, on average, from bulgeless to bulgy galaxies (see Table 3), that

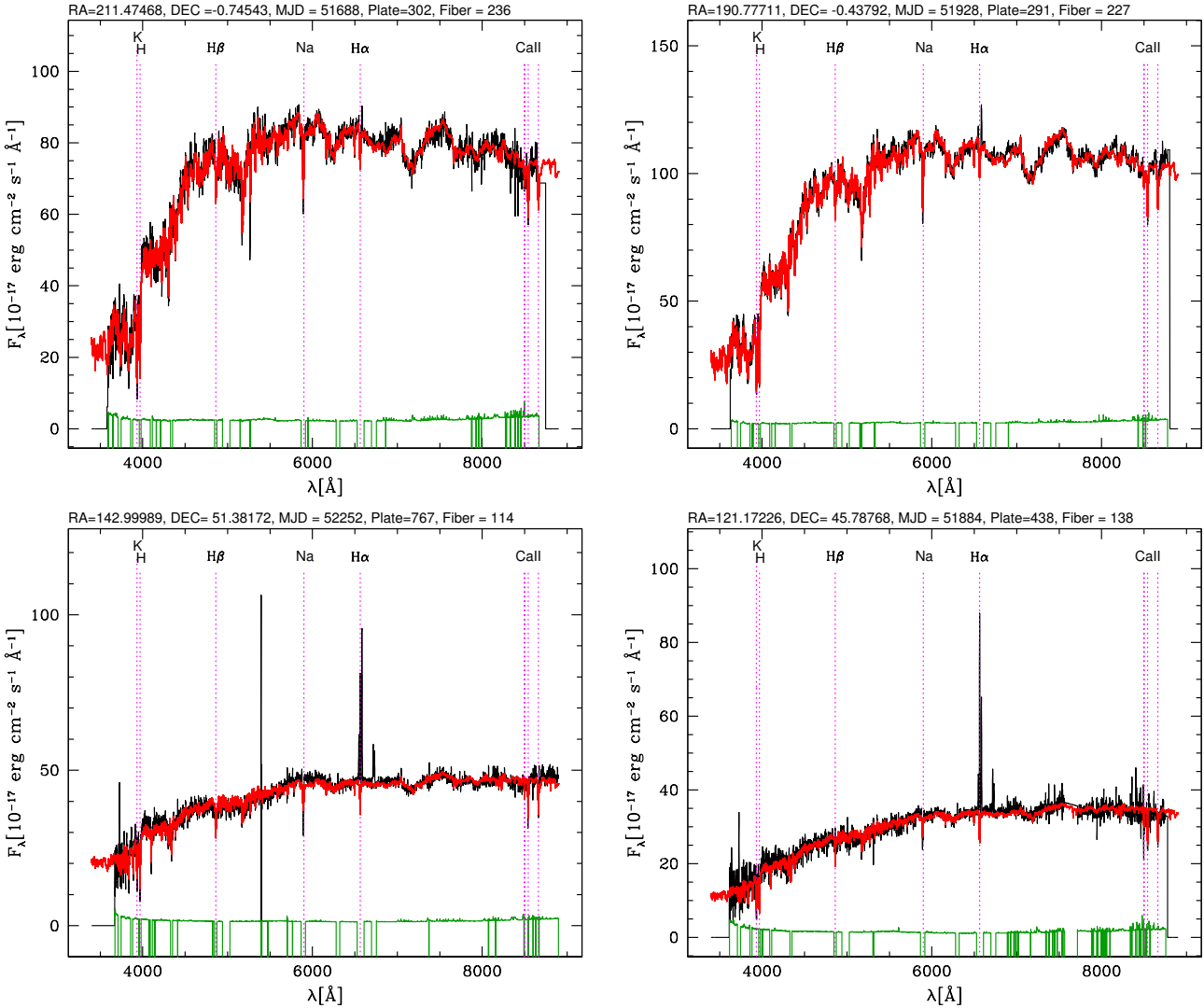


Figure 6. SDSS spectra in rest-frame and corrected for Galactic extinction using the dust maps from Schlegel et al. (1998) with additional corrections described in Schlafly & Finkbeiner (2011). In each panel, the observed spectrum is in black, the red curve combines the 50 fits from STARLIGHT and green is the error spectrum (where negative values indicate wavelengths masked prior to the fit due to spurious pixels and/or emission lines). Each of the 4 classes is represented here: bulgy (top left), intermediate (top right), pseudo-bulge (bottom left) and bulgeless (bottom right).

likely follows the similar increase in the bulge luminosity (see Table 2).

4.3 Kinematics of the central regions

We have further investigated whether any of our structural classes deviates from the Faber-Jackson relation (Faber & Jackson 1976, hereafter FJ) for classical bulges and early-type galaxies. To this end, we adopted as reference the relation by La Barbera et al. (2010) who analyzed a sample of $\sim 40\,000$ nearby early-type galaxies by fitting the relation $\log \sigma_* = \lambda_0 + \lambda_1 \times (\log L + 0.4X)$ for the grizYJHK photometric bands, where σ_* is the stellar velocity dispersion and L the galaxy luminosity in the respective band. These authors have obtained the linear regression coefficients λ_0 and λ_1 for the FJ relation after assuming a magnitude limit X in the corresponding wavebands. For the SDSS r-band, the mag-

nitude limit and coefficients they derived are $X = -20.60$, $\lambda_0 = 2.151 \pm 0.008$ and $\lambda_1 = 0.192 \pm 0.018$.

After plotting the logarithm of σ_* (obtained through STARLIGHT) as a function of the total absolute magnitude for our sample galaxies, we added the La Barbera et al. (2010) FJ relation (thick magenta line in Fig. 9). Bulgy galaxies seem to follow the relation quite well whereas pseudo-bulges and disks are located systematically below it, in agreement with the trends suggested by Kormendy & Kennicutt (2004) and also observed by e.g. Zhao (2012) for a particular sample of 75 bulges in isolated Sb-Sc SDSS nearby spiral galaxies. In our work, we are aware that we cannot use σ_* as a “clean” measure of the velocity dispersion in the central region of bulgeless and pseudo-bulge galaxies because we expect these systems to show a significant degree of rotational support, at variance with pressure-supported classical bulges. Therefore, σ_* has to be seen as an upper-limit to the true stellar velocity

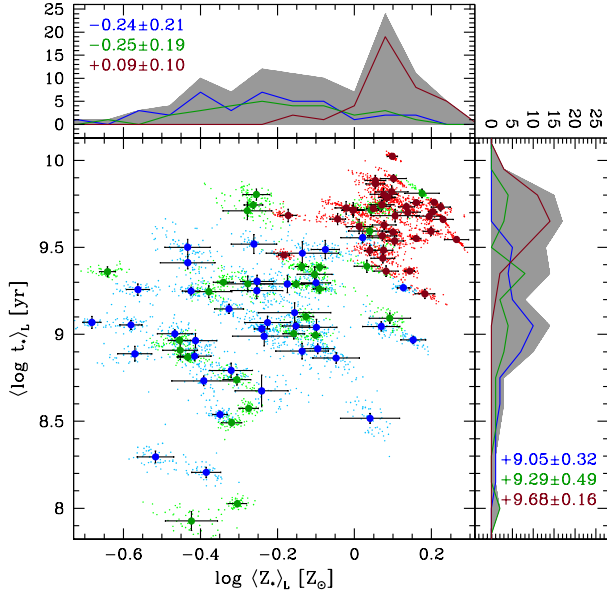


Figure 7. Mean stellar metallicity $\langle Z_{\star} \rangle_L$ (in solar units) versus mean stellar age $\langle \log t_{\star} \rangle_L$, both luminosity-weighted, for bulgeless (blue), pseudo-bulge (green) and bulgy (red) galaxies (we note this class henceforth merges all $\eta_b > 1.5$ galaxies, irrespective of having a disk or not). For each galaxy, the 50 STARLIGHT individual runs are shown as small dots, while the large filled circle corresponds to the median value with 1σ (standard deviation) error bars. Histograms are also shown for each class (same color coding): on the top panel for $\langle Z_{\star} \rangle_L$, and on the right-hand-side panel for $\langle \log t_{\star} \rangle_L$; the grey shaded area depicts the total distribution of our galaxy sample. The small colored numbers in each histogram panel are the median values, with 1σ , for each structural class (with the same respective color coding). The y-axis values represent the number of galaxies.

dispersion in these systems, which should only reinforce the result we obtained. Finally, it is worth pointing out that pseudo-bulges tend to lie in the intermediate region between pure disks and bulgy galaxies, as evidenced by the median values of the distributions - large squares in Fig. 9 and Table 3. Taken in combination with the previous results on stellar ages, metallicity and stellar masses, one might infer that pseudo-bulges and the centers of bulgeless galaxies possibly share a similar formation pathway, which is distinct from the one driving the rapid growth and settlement of classical bulges on the FJ relation.

4.4 Emission-lines and line ratios

As mentioned in section 3, emission-lines were measured after subtraction of the best-fitting stellar continuum model. Note that this procedure was repeated 50 times for each SDSS spectrum, due to the multiple STARLIGHT fits obtained. Quite importantly, not in all 50 trials were we able to measure the emission-lines, especially for bulgy galaxies where nebular emission is generally very faint.

Table 3 shows that A_V , the V-band extinction determined from models with STARLIGHT, is remarkably distinct for the different classes: there seems to be a dichotomy, separating bulgeless/pseudo-bulges from bulgy galaxies. The for-

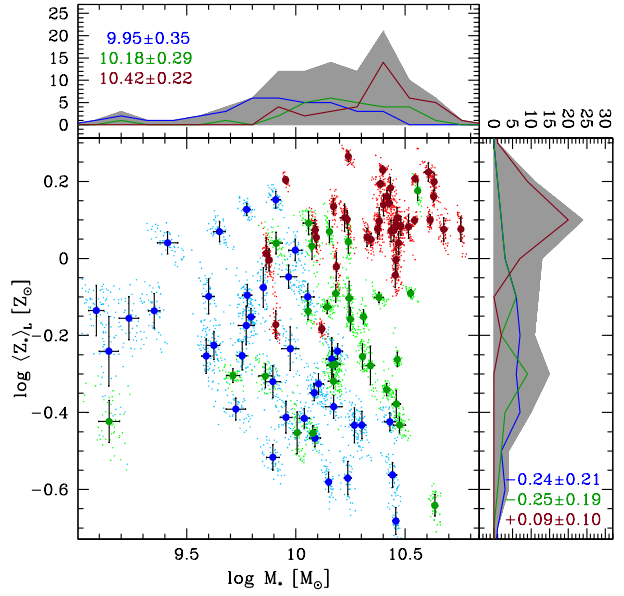


Figure 8. Logarithm of the total presently available stellar mass (i.e. the stellar mass ever formed, after correction for the fraction of returned mass into the ISM) as a function of the light-weighted mean stellar metallicity. This diagram delineates a trend similar to the Tremonti et al. (2004) mass-metallicity relation, but with respect to the stellar values and only using our sample of red galaxies. Symbols, color coding and overall structure of this figure are as in Fig. 7.

mer also span a similar distribution with regard to the gas-phase extinction, inferred through the Balmer decrement $H\alpha/H\beta$, with typical values higher than 2.86 (the theoretical value for these recombination lines in HII regions for typical conditions) and being clearly separated from bulgy galaxies. Both parameters (A_V and Balmer decrement) are obviously correlated and their values lead us to infer that the centers of pseudo bulges and disk galaxies are more dust-enriched than classical bulges.

In order to further investigate the star formation activity of our sample galaxies we have derived the classical Baldwin et al. (1981, hereafter BPT) diagram to classify optical emission-line spectra into HII/Star-Forming (SF), Composites and LINER/Seyfert galaxies using the $[NII]\lambda 6583/H\alpha$ versus $[OIII]\lambda 5007/H\beta$ emission-line ratios (see Fig. 10). The adopted demarcation lines are from Kauffmann et al. (2003, hereafter Ka03) to select SF galaxies, and the theoretical upper limit obtained from photoionization models proposed by Kewley et al. (2001, hereafter Ke01) to separate star-forming from other ionization sources such as shocks, post-AGB stars and AGNs. In order to discriminate Seyferts from LINERs, we adopted the Schawinski et al. (2007, hereafter Sc07) demarcation line.

In terms of the ionization properties, we can clearly see a sequence where star-forming galaxies tend to be bulgeless, pseudo-bulges are mainly composites (though there is a large dispersion) and bulgy commonly lie in the LINER regime. Since disk and pseudo-bulges are found preferentially below the Ke01 demarcation line, we can conclude that there is still ongoing star-formation activity, while ex-

Table 3. Median and dispersion (standard deviation) values of several parameters obtained from fitting STARLIGHT models to SDSS spectra that gather the emission within the inner $3''$ of each sample galaxy. Columns give, for each structural class now considered: mean stellar metallicity (in solar units); mean stellar age (in years); stellar mass (in solar units) corrected for the mass returned to the ISM due to stellar winds and SNe explosions; V-band extinction; velocity dispersion of stellar absorption lines (in km/s); emission line ratios $[\text{NII}]\lambda 6583/\text{H}\alpha$, $[\text{OIII}]\lambda 5007/\text{H}\beta$ and $\text{H}\alpha/\text{H}\beta$.

Structural class	$\log \langle Z_* \rangle_L$	$\log \langle \log t_* \rangle_L$	$\log M_*$	A_V	σ_*	$\log [\text{NII}]/\text{H}\alpha$	$\log [\text{OIII}]/\text{H}\beta$	$\log \text{H}\alpha/\text{H}\beta$
bulgeless galaxies	-0.24 ± 0.21	9.05 ± 0.32	9.95 ± 0.35	0.74 ± 0.37	74.5 ± 27.5	-0.36 ± 0.10	-0.38 ± 0.32	0.79 ± 0.13
pseudo-bulge galaxies	-0.25 ± 0.19	9.29 ± 0.49	10.18 ± 0.29	0.84 ± 0.39	108.2 ± 33.2	-0.17 ± 0.18	-0.18 ± 0.37	0.80 ± 0.27
bulgy galaxies	$+0.09 \pm 0.10$	9.68 ± 0.16	10.42 ± 0.22	0.03 ± 0.08	160.5 ± 41.0	0.07 ± 0.17	0.13 ± 0.17	0.32 ± 0.32

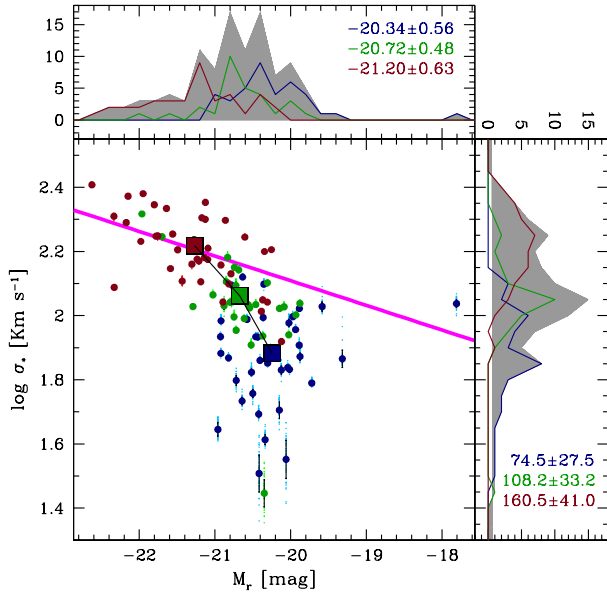


Figure 9. Logarithm of the stellar velocity dispersion (in km s^{-1}) within the central region as a function of the total r-band magnitude (computed with GALFIT) for all galaxies belonging to the three classes now considered. Symbols and colors are as before (Figs. 7, 8); but velocity dispersion values on the right panel are given directly in km/s , and we’ve now added large squares to mark, for each structural class, the median value of the parameter under study (as in Table 3). The thick magenta line shows the Faber-Jackson (FJ) relation from La Barbera et al. (2010) for early-type local galaxies. We can clearly see that bulgy galaxies fall within that relation, having a median value of -21.20 mag in the r-band and a mean velocity dispersion of ~ 161 km/s . On the other hand, bulgeless and pseudo-bulges deviate strongly from the FJ relation.

tra sources of ionization have to be invoked in bulgy systems to explain their emission-line ratios, and only residual star-formation might be in place. This is compatible with the hypothesis of disk/pseudo-bulges building up in the course of secular galaxy evolution, in contrast to bulgy galaxies that have formed the bulk of their stars much earlier and presently exhibit very low, if any at all, star-formation activity. It also shows that our selection minimizes occurrence of star-forming objects in our sample⁶ but does not exclude

⁶ As described in section 2, galaxy g-r SDSS colors are red: mean values range from 0.75 to 0.81 for the different classes of table

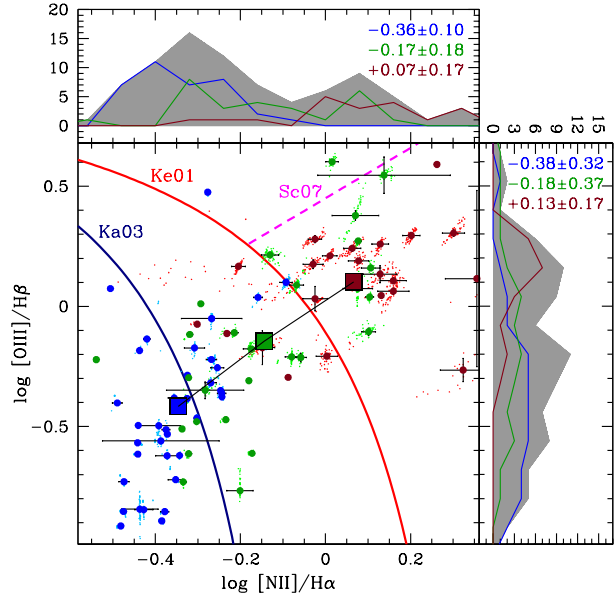


Figure 10. BPT emission-line ratio diagnostic diagram for $[\text{NII}]\lambda 6583/\text{H}\alpha$ versus $[\text{OIII}]\lambda 5007/\text{H}\beta$. The demarcation lines in blue, red and magenta are the ones proposed by Kauffmann et al. (2003, Ka03), Kewley et al. (2001, Ke01) and Schawinski et al. (2007, Sc07), respectively. They are used to classify galaxies according to the ionization source: Ke01 is a theoretical upper limit from stellar photoionization models, while Ka03 is used for demarcating star-forming galaxies; Sc07 is used to separate between Seyfert and LINER regimes. Symbols are as before (see Fig. 9).

them completely, as expected. Noteworthy is also that, despite being intrinsically red in terms of having a dominantly aged, red stellar population, some star formation is taking place in these bulgeless and pseudo-bulge galaxies - enough to produce the gas excitation we observe. These situations, however, are not a problem for this work since the generally very faint nebular emission in these systems should not lead to any bias on our results, while rendering confidence to our morphological classification and SPS results.

1, being rather typical of early-types (e.g. Fukugita et al. 1995). Individual galaxy colors are given in tables A1-A4. Visual inspection of the images, also described in section 2, further concurred to eliminate objects with characteristics indicative of significant star formation.

4.5 Mass assembly history of galaxies

An important insight that can be gained from spectral synthesis models is the mass assembly history (MAH, e.g. Heavens et al. 2004; Asari et al. 2007; McDermid et al. 2015), i.e. the cumulative stellar mass fraction as a function of time, here determined within the central $3''$ of the analyzed galaxies (Fig. 11). The curves were obtained from the STARLIGHT star formation histories of galaxies and smoothed to 0.5 dex. The statistics include the 50 different STARLIGHT runs for each galaxy in our sample and we highlight the median trend for each structural class (bulgeless, pseudo-bulge and bulgy). Since we have selected red galaxies from the SDSS, we expect that the bulk of their stellar mass was formed rather early-on for all distinct categories. Analyzing the curves in figure 11, we see that the assembly of the stellar mass within the galaxy centers was accomplished more than 1 Gyr ago for our three classes. However, the pace at which each structural class assembles its central stellar mass is different, being slower in bulgeless, moderate in pseudo-bulges and faster in bulgy galaxies. The large filled squares mark the corresponding MAH values at an age of the Universe of ~ 7.7 Gyr where bulgeless galaxies have assembled 80% of their inner stellar mass, while pseudo-bulge and bulgy galaxies have already formed 89% and 93% of their fiber stellar mass, respectively.

These results seem to be compatible with the secular evolution scenario for pseudo-bulges, pointing to prolonged star forming activity that is fed by gas inflow from the disk or the halo, leading to a gradual build-up of the (pseudo)bulge at a slower pace. This star formation is a process still ongoing, as demonstrated in the last section. It is worth reiterating that, despite our optical color selection criteria, some of these galaxies have emission lines reflecting ongoing star formation in a moderately dusty environment in their central regions. This star formation seems to be relevant in light but probably not so much in the percentage of central stellar mass formed: being enough to place them in the BPT parameter space typical of HII regions and alike, and contributing to secularly building-up the inner regions of these galaxies and the growth of the pseudo-bulge, it does not increase significantly the amount of stellar mass already present - at least in the last Gyr.

On the other hand, classical bulges seem to assemble their stellar mass at a much faster rate, in a process consistent with a violent galaxy merger or rapid gas collapse scenario. Additionally, they show no signs of significant recent star-formation activity in their centers, consist of old stellar populations only, and likely have almost no gas left to fuel star formation. Our results are compatible with those obtained by Zhao 2012 through spectral fitting of bulges and pseudo-bulges in 75 isolated late-type galaxies located at lower redshift than our sample. This study concluded that either class has formed most of its stellar mass ~ 10 Gyr ago, with the important difference of pseudo-bulges sustaining star-forming activity over a longer timescale than classical ones, in qualitative agreement with the secular evolution scenario.

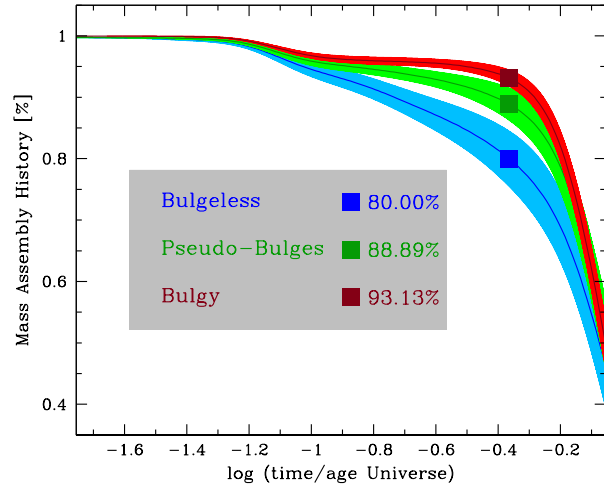


Figure 11. Mass assembly history (MAH) as a function of lookback time, normalized to the age of the Universe, for our different structural classes: bulgeless (blue), pseudo-bulges (green) and bulgy galaxies (red). Each curve shows the median trend for each galaxy class under consideration, with the same color shading showing the dispersion of the values (including the multiple STARLIGHT runs for each galaxy). Since this sample consists of optically red galaxies, the bulk of their stellar mass was formed more than 1 Gyr ago. However, the pace at which each class assembles its stellar mass is different, being slower in bulgeless, moderate in pseudo-bulges and faster in bulgy galaxies. The large filled squares mark the corresponding MAH values for an age of the Universe of ~ 7.7 Gyr (~ 6 Gyr in lookback time) when bulgeless galaxies have assembled 80% of their central stellar mass, while pseudo-bulge and bulgy galaxies have already formed $\sim 89\%$ and $\sim 93\%$ of their stellar mass (also in the inner $3''$), respectively.

4.6 Discussion on possible aperture biases

One should consider whether aperture effects might be inducing the trends unveiled by the population synthesis analysis. The fixed SDSS fiber aperture implies that, for higher redshift galaxies, the area probed by the spectra is physically larger (we recall it ranges from ~ 1.2 to ~ 3.4 kpc, in diameter, for our sample). We must then quantify, for galaxies having a disk+bulge structure, if their fiber spectra is contaminated by disk light. Fig. 1 shows that the redshift distributions are quite similar, especially among galaxies having a bulge, so one would not expect the above hypothesis to have any impact on the observed tendencies. In any case, we have made some tests so as to be sure that our results concerning pseudo-bulges, and their apparent similarity with disks in several properties, are not driven by aperture effects.

Following Zhao (2012, see also references therein), we computed the flux contribution provided by disk and bulge inside a region with radius $1.5''$ (respectively, $F_d(< 1.5'')$ and $F_b(< 1.5'')$), the size of SDSS fibers. These quantities are computed analytically from the integral of the Sérsic function using the parameters obtained with GALFIT. Results for the ratio $r_{1.5} = F_b(< 1.5'')/F_d(< 1.5'') \equiv L_b(< 1.5'')/L_d(< 1.5'')$ are shown in Fig. 12 for the two classes having a disk+bulge structure (i.e. pseudo-bulge galaxies and intermediate- η ones). In the figure, we also mark the limit where the light from the bulge is about 6 times more than that from the disk within the $1.5''$ radius aperture;

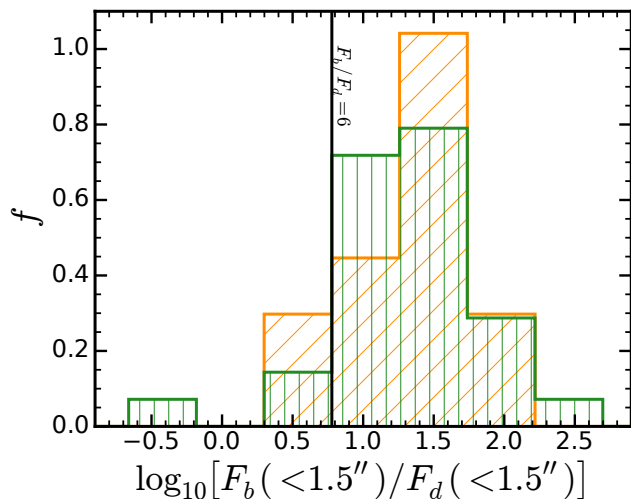


Figure 12. Normalized histogram of the bulge-to-disk flux ratio inside the fiber aperture computed from the best fit models derived with GALFIT. The green histogram refers to pseudo-bulge galaxies, while the orange histogram shows values for the intermediate- η bulge galaxies. The vertical black solid line refers to the limit for bulge dominance defined in Zhao (2012).

below this line lie objects where the disk contribution becomes important for the light collected by the SDSS fiber (Zhao 2012). As most of our sample is above this limit, this clearly hints to aperture effects not being an issue in our sample: we thus expect that the parameters inferred from SPS for pseudo-bulges are not contaminated by the light of the underlying disk of the host galaxy.

5 SUMMARY AND CONCLUSIONS

This article presents a comparative study of bulgeless, pseudo-bulge and *bulgy* (classical-bulge and early-type) galaxies with respect to the star formation history, stellar velocity dispersion, metallicity and gas-excitation mechanisms in their central part. Our main goal is to obtain further observational constraints on the question of whether pseudo-bulges are distinct from classical bulges in terms of their assembly history, as expected by the secular growth scenario for the former.

Our sample was deliberately selected such as to comprise undistorted low-inclination galaxies with spectrophotometric properties indicative of negligible levels of both ongoing star-forming activity and intrinsic obscuration by dust. This ensures a reliable morphological analysis and classification, and that the spectral fitting analysis of SDSS spectra is unbiased, thereby allowing for a robust comparison of the physical and evolutionary characteristics of the above classes. The latter were defined on the basis of the structural properties of our sample galaxies, as obtained through 2D bulge/disk image decomposition with GALFIT, and by demanding a minimum Sérsic index $\eta > 1.5$ for classical bulges. The redshift range of our sample ensures that the region probed by the SDSS fiber is adequate for sampling the stellar populations of the bulge without significant contamination from the underlying disk, which is an improvement on previous studies (Zhao 2012). Our sample

(106 galaxies) comprises nearly equal parts of bulgeless (38), pseudo-bulge (29) and bulgy (39) systems, in an attempt to increase the number of objects under study relatively to previous works related with this topic (eg Moorthy & Holtzman 2006; MacArthur et al. 2009; Zhao 2012). Furthermore, a cut in stellar mass aims at avoiding introducing any strong dependence on this parameter by excluding low-mass galaxies.

The main results from this study may be summarized as follows:

- Our photometric analysis suggests that disks underlying pseudo-bulges typically have larger exponential scale lengths than bulgeless galaxies, despite similar integral disk luminosities. One can try to elaborate on whether this is related to the build up of the pseudo-bulge mass. Models of pseudo-bulge growth via satellite accretion (such as the ones explored by e.g. Eliche-Moral et al. 2006) show that these events lead to an increase of the disk scale length that depends on the mass of the satellite. This occurs due to the outward transport of disk material in the outer regions, combined with inward transport to the bulge in the inner regions. However, the very same physical argument (outward transfer of angular momentum) is also used to justify the expansion of galaxy disks and accompanying concentration in the inner regions, leading to bulge growth, but in the framework of secular evolution (see e.g. Kormendy & Kennicutt 2004 and also Sachdeva et al. 2015 and references to models therein). The results from our study *per se* do not permit discrimination between these two scenarios.

- Spectral synthesis models of the stellar emission within the SDSS fiber aperture reveal a clear segregation of bulgeless and pseudo-bulge galaxies from bulgy ones with respect to the luminosity-weighted age (t_*) vs metallicity (Z_*): Notwithstanding a large dispersion among galaxies within a class, the former two classes were found to significantly differ (median of <2 Gyr and $0.6 Z_\odot$, respectively) from classical bulges (~ 5 Gyr and $1.2 Z_\odot$, respectively). This contrasts with previous results: Moorthy & Holtzman (2006); MacArthur et al. (2009); Zhao (2012) find that pseudo and classical bulges do not have significantly different stellar populations. However, samples are selected in a noticeably different way and some of these works have very few objects, whereas a large scatter is present also in our case.

- On the stellar mass (M_*) vs Z_* plane, classical bulges predominantly populate the high-mass, high-metallicity locus ($M_* \gtrsim 10^{10} M_\odot$ and $Z_* \gtrsim Z_\odot$), whereas pseudo-bulges and the central regions of disks span a wide range of values, from partial overlap with the former to ~ 1 dex lower M_* and reaching down to subsolar metallicities of $\sim Z_\odot/4$.

- Still within their central regions, bulgeless galaxies and pseudo-bulges show a clear tendency for a higher gas-phase metallicity than bulgy systems, a fact pointing to a substantially different chemical enrichment (and star formation) history. This is also reflected on the stellar mass assembly histories derived in this study, indicating a gradual, gentler rise of stellar mass from bulgy towards bulgeless systems: at a look-back time of ~ 6 Gyr, the percentage of the present-day stellar mass at the centers of bulgeless, pseudo-bulge and bulgy has been determined to be 80%, 89% and 93%, respectively. This indicates that, whereas the stellar mass in all analyzed systems is predominantly old (presumably due to our particular selection criteria), the former two classes

have undergone significant star-forming activity and stellar mass growth over the past few Gyrs.

- Whereas bulge systems were found to closely obey the Faber-Jackson relation, the centers of bulgeless and pseudo-bulges are systematically underluminous (by up to ~ 2.5 mag) in the r-band at a given stellar velocity dispersion σ_* . Given the increased importance of rotational motions in pseudo-bulges, their inferred σ_* is rather an upper limit, which further underscores their kinematic departure from the Faber-Jackson relation for classical bulges and early-type galaxies.

- An analysis of diagnostic emission-line ratios reveals a systematic trend along the bulgeless \rightarrow pseudo-bulge \rightarrow bulgy sequence, further highlighting the diverse nature of these entities: whereas BPT ratios for bulgeless galaxies are mostly compatible with those for HII regions, those for pseudo-bulges suggest a broad range of gas excitation mechanisms, from star formation all the way to AGN. Bulgy galaxies, on the other hand, are almost exclusively found within the LINER regime of BPT diagrams.

Our results thus show that some trends hold for the central regions of galaxies (from bulgeless to bulgy) concerning specific parameters inferred from the morphological and SPS analysis. And such relations seem to indicate that pseudo-bulges occupy a transition region between these two in several parameter spaces. Namely, the fact that pseudo-bulges seem to have residual star formation, younger stellar populations and, consistently, a more prolonged stellar mass assembly history than classical (bulgy) systems, lends strong support to the notion that the central bulge-like component is forming secularly in these galaxies. On the other hand, the determined disk scale length of pseudo-bulge galaxies could, in principle, be compatible with both models (secular evolution or rapid processes such as minor mergers). Though the majority of our results thus favor the more commonly accepted scenario of different formation mechanisms between pseudo-bulges and classical ones, it is far from straightforward to exclude other possibilities, and a complex picture for the assembly of these structures seems more reasonable as evidence builds up.

ACKNOWLEDGMENTS

JMG acknowledges support by Fundação para a Ciência e a Tecnologia (FCT) through the Fellowship SFRH/BPD/66958/2009 and POPH/FSE (EC) by FEDER funding through the program Programa Operacional de Factores de Competitividade (COMPETE). PP is supported by FCT through the Investigador FCT Contract No. IF/01220/2013 and POPH/FSE (EC) by FEDER funding through the program COMPETE. JMG&PP also acknowledge support by FCT under project FCOMP-01-0124-FEDER-029170 (Reference FCT PTDC/FIS-AST/3214/2012), funded by FCT-MEC (PIDDAC) and FEDER (COMPETE). This work was supported by Fundação para a Ciência e a Tecnologia (FCT) through the research grant UID/FIS/04434/2013.

It is a pleasure to acknowledge M. Taylor for developing TOPCAT (<http://www.starlink.ac.uk/topcat/>).

M. Blanton is acknowledged for support concerning the NYU-VAGC usage.

Funding for the SDSS and SDSS-II has been provided by the Alfred P. Sloan Foundation, the Participating Institutions, the National Science Foundation, the U.S. Department of Energy, the National Aeronautics and Space Administration, the Japanese Monbukagakusho, the Max Planck Society, and the Higher Education Funding Council for England. The SDSS Web Site is <http://www.sdss.org/>.

The SDSS is managed by the Astrophysical Research Consortium for the Participating Institutions. The Participating Institutions are the American Museum of Natural History, Astrophysical Institute Potsdam, University of Basel, University of Cambridge, Case Western Reserve University, University of Chicago, Drexel University, Fermilab, the Institute for Advanced Study, the Japan Participation Group, Johns Hopkins University, the Joint Institute for Nuclear Astrophysics, the Kavli Institute for Particle Astrophysics and Cosmology, the Korean Scientist Group, the Chinese Academy of Sciences (LAMOST), Los Alamos National Laboratory, the Max-Planck-Institute for Astronomy (MPIA), the Max-Planck-Institute for Astrophysics (MPA), New Mexico State University, Ohio State University, University of Pittsburgh, University of Portsmouth, Princeton University, the United States Naval Observatory, and the University of Washington.

This research has made use of the NASA/IPAC Extragalactic Database (NED) which is operated by the Jet Propulsion Laboratory, California Institute of Technology, under contract with the National Aeronautics and Space Administration.

REFERENCES

- Alongi M., Bertelli G., Bressan A., Chiosi C., Fagotto F., Greggio L., Nasi E., 1993, *A&AS*, 97, 851
- Asari N. V., Cid Fernandes R., Stasińska G., Torres-Papaqui J. P., Mateus A., Sodré L., Schoenell W., Gomes J. M., 2007, *MNRAS*, 381, 263
- Baldwin J. A., Phillips M. M., Terlevich R., 1981, *PASP*, 93, 5
- Bamford S. P., et al., 2009, *MNRAS*, 393, 1324
- Barentine J. C., Kormendy J., 2012, *ApJ*, 754, 140
- Bell E. F., 2008, *ApJ*, 682, 355
- Bennert V. N., Treu T., Auger M. W., Rosen R., Harris C. E., Malkan M. A., Woo J.-H., 2014, preprint, ([arXiv:1409.4428](https://arxiv.org/abs/1409.4428))
- Blanton M. R., et al., 2005, *AJ*, 129, 2562
- Bressan A., Fagotto F., Bertelli G., Chiosi C., 1993, *A&AS*, 100, 647
- Bruzual G., Charlot S., 2003, *MNRAS*, 344, 1000
- Cardelli J. A., Clayton G. C., Mathis J. S., 1989, *ApJ*, 345, 245
- Chabrier G., 2003, *PASP*, 115, 763
- Cid Fernandes R., Mateus A., Sodré L., Stasińska G., Gomes J. M., 2005, *MNRAS*, 358, 363
- Ciotti L., Bertin G., 1999, *A&A*, 352, 447
- Coelho B., Antón S., Lobo C., Ribeiro B., 2013, *MNRAS*, 436, 2426
- Combes F., Debbasch F., Friedli D., Pfenniger D., 1990, *A&A*, 233, 82
- Eliche-Moral M. C., Balcells M., Aguerri J. A. L., González-García A. C., 2006, *A&A*, 457, 91

- Eliche-Moral M. C., González-García A. C., Balcells M., Aguerri J. A. L., Gallego J., Zamorano J., Prieto M., 2011, *A&A*, 533, A104
- Erwin P., et al., 2015, *MNRAS*, 446, 4039
- Faber S. M., Jackson R. E., 1976, *ApJ*, 204, 668
- Fagotto F., Bressan A., Bertelli G., Chiosi C., 1994a, *A&AS*, 104, 365
- Fagotto F., Bressan A., Bertelli G., Chiosi C., 1994b, *A&AS*, 105, 29
- Fernández Lorenzo M. e. a., 2014, *ApJL*, 788, L39
- Fisher D. B., Drory N., 2008, *AJ*, 136, 773
- Fisher D. B., Drory N., 2011, *ApJ*, 733, L47
- Fisher D. B., Drory N., Fabricius M. H., 2009, *ApJ*, 697, 630
- Fukugita M., Shimasaku K., Ichikawa T., 1995, *PASP*, 107, 945
- Gadotti D. A., 2009, *MNRAS*, 393, 1531
- Gelman A., Rubin D. B., 1992, *Statist. Sci.*, 7, 457
- Girardi L., Bressan A., Chiosi C., Bertelli G., Nasi E., 1996, *A&AS*, 117, 113
- Guedes J., Mayer L., Carollo M., Madau P., 2013, *ApJ*, 772, 36
- Guo Y., et al., 2009, *MNRAS*, 398, 1129
- Heavens A., Panter B., Jimenez R., Dunlop J., 2004, *Nature*, 428, 625
- Hopkins P. F., et al., 2010, *ApJ*, 715, 202
- Kauffmann G., et al., 2003, *MNRAS*, 346, 1055
- Kehrig C. e. a., 2012, *A&A*, 540, A11
- Keselman J. A., Nusser A., 2012, *MNRAS*, 424, 1232
- Kewley L. J., Dopita M. A., Sutherland R. S., Heisler C. A., Trevena J., 2001, *ApJ*, 556, 121
- Kormendy J., Kennicutt Jr. R. C., 2004, *ARA&A*, 42, 603
- Kormendy J., Drory N., Bender R., Cornell M. E., 2010, *ApJ*, 723, 54
- Kubryk M., Prantzos N., Athanassoula E., 2013, *MNRAS*, 436, 1479
- La Barbera F., de Carvalho R. R., de La Rosa I. G., Lopes P. A. A., 2010, *MNRAS*, 408, 1335
- Larson D. e. a., 2011, *ApJS*, 192, 16
- MacArthur L. A., González J. J., Courteau S., 2009, *MNRAS*, 395, 28
- Masters K. L., et al., 2010, *MNRAS*, 405, 783
- McDermid R. M., et al., 2015, *MNRAS*, 448, 3484
- Mendez-Abreu J., Debattista V. P., Corsini E. M., Aguerri J. A. L., 2014, preprint, ([arXiv:1409.2876](https://arxiv.org/abs/1409.2876))
- Moorthy B. K., Holtzman J. A., 2006, *MNRAS*, 371, 583
- Morelli L., et al., 2008, *MNRAS*, 389, 341
- Naab T., Trujillo I., 2006, *MNRAS*, 369, 625
- Okamoto T., 2013, *MNRAS*, 428, 718
- Peng C. Y., Ho L. C., Impey C. D., Rix H.-W., 2002, *AJ*, 124, 266
- Peng C. Y., Ho L. C., Impey C. D., Rix H.-W., 2010, *AJ*, 139, 2097
- Querejeta M., Eliche-Moral M. C., Tapia T., Borlaff A., Rodríguez-Pérez C., Zamorano J., Gallego J., 2014, preprint, ([arXiv:1409.5126](https://arxiv.org/abs/1409.5126))
- Sachdeva S., Gadotti D. A., Saha K., Singh H. P., 2015, preprint, ([arXiv:1504.06218](https://arxiv.org/abs/1504.06218))
- Schawinski K., Thomas D., Sarzi M., Maraston C., Kaviraj S., Joo S.-J., Yi S. K., Silk J., 2007, *MNRAS*, 382, 1415
- Schlafly E. F., Finkbeiner D. P., 2011, *ApJ*, 737, 103
- Schlegel D. J., Finkbeiner D. P., Davis M., 1998, *ApJ*, 500, 525
- Sérsic J. L., 1968, *Atlas de galaxies australes*
- Simard L., Mendel J. T., Patton D. R., Ellison S. L., McConnell A. W., 2011, *ApJS*, 196, 11
- Ueda J., et al., 2014, *ApJS*, 214, 1
- Wadadekar Y., Robbason B., Kembhavi A., 1999, *AJ*, 117, 1219
- Zhao Y., 2012, *Ap&SS*, 337, 719

APPENDIX A: APPENDIX: TABLES WITH GALAXY PROPERTIES

Table A1. Table with general properties and structural parameters (as defined in equation 2) for the pseudo-bulge galaxies studied in this paper. Columns are as follows: (1) and (2) give the J2000 coordinates of the galaxies (in degrees); (3) SDSS redshift value; (4) $g-r$ color from the NYU-VAGC catalog; (5) Total r-band magnitude of the galaxy as derived from GALFIT; (6) and (7) Effective radii, in kpc, of the structural components, disk and bulge respectively; (8) The Sérsic index of the bulge component; (9) The morphological class assigned to the galaxy (as in Table 1).

α (J2000)	δ (J2000)	z	$g-r$	$M_{r,tot}$	$r_{e,d}$	$r_{e,b}$	η_b
212.9395	-0.9043	0.0544	0.8190	-20.46	9.93 ± 0.21	1.79 ± 0.02	0.68 ± 0.02
130.7137	52.9251	0.0591	0.8103	-20.74	6.22 ± 0.13	1.70 ± 0.03	0.62 ± 0.04
220.8427	1.0981	0.0381	0.7261	-21.03	4.53 ± 0.03	1.54 ± 0.02	0.58 ± 0.02
322.7421	-7.0855	0.0278	0.8528	-20.75	6.23 ± 0.05	1.16 ± 0.01	0.74 ± 0.01
30.7166	-8.0267	0.0335	0.8086	-20.56	5.98 ± 0.04	1.11 ± 0.01	0.95 ± 0.01
25.9110	13.5277	0.0542	0.8705	-20.69	14.12 ± 0.24	1.62 ± 0.01	0.46 ± 0.02
131.1434	46.8706	0.0522	0.7995	-20.09	7.68 ± 0.32	2.13 ± 0.05	0.74 ± 0.02
142.9998	51.3818	0.0333	0.6995	-20.37	3.91 ± 0.07	1.28 ± 0.03	1.09 ± 0.02
194.6264	63.7096	0.0397	0.8460	-19.93	5.28 ± 0.08	0.97 ± 0.01	0.62 ± 0.04
221.8257	58.2260	0.0375	0.7759	-20.52	3.64 ± 0.02	1.70 ± 0.02	0.42 ± 0.02
254.4245	33.9194	0.0597	0.8135	-19.88	9.36 ± 0.20	1.57 ± 0.02	1.01 ± 0.03
117.8212	32.7403	0.0557	0.7645	-20.72	5.16 ± 0.06	1.39 ± 0.02	0.34 ± 0.04
155.1420	7.8518	0.0441	0.8683	-20.31	5.47 ± 0.08	1.04 ± 0.01	0.81 ± 0.02
162.9716	8.8632	0.0523	0.7222	-20.75	7.20 ± 0.13	1.86 ± 0.03	0.80 ± 0.03
231.4910	48.2958	0.0361	0.7062	-20.35	4.42 ± 0.03	2.22 ± 0.03	1.46 ± 0.01
145.2456	40.0365	0.0412	0.8357	-20.02	5.40 ± 0.07	0.81 ± 0.01	0.33 ± 0.02
158.9306	12.2550	0.0495	0.8860	-20.78	8.84 ± 0.16	1.96 ± 0.02	0.73 ± 0.02
188.8515	47.6891	0.0454	0.9074	-20.15	4.58 ± 0.08	0.92 ± 0.01	0.86 ± 0.02
253.8737	23.3854	0.0553	0.9055	-21.29	10.46 ± 0.07	1.12 ± 0.02	0.70 ± 0.06
237.9711	27.2427	0.0589	0.7937	-20.72	6.11 ± 0.09	1.43 ± 0.01	0.42 ± 0.02
19.6423	-0.2283	0.0472	0.7822	-20.85	5.90 ± 0.05	1.38 ± 0.01	0.35 ± 0.01
18.7512	0.0309	0.0497	0.7580	-20.54	5.22 ± 0.09	0.96 ± 0.01	0.86 ± 0.02
197.9124	34.6365	0.0374	0.8359	-20.88	5.35 ± 0.04	5.49 ± 0.06	1.21 ± 0.01
151.1738	28.3567	0.0516	0.9225	-20.83	7.58 ± 0.06	0.88 ± 0.01	0.54 ± 0.03
135.5952	14.5252	0.0301	0.8168	-21.27	14.23 ± 0.16	2.66 ± 0.01	0.82 ± 0.01
168.9758	20.7440	0.0599	0.7755	-20.80	8.71 ± 0.11	1.97 ± 0.01	1.00 ± 0.01
174.4652	21.9742	0.0303	0.7217	-21.96	12.86 ± 0.13	1.71 ± 0.00	1.31 ± 0.01
223.5155	18.4004	0.0571	0.8136	-20.61	5.12 ± 0.06	1.65 ± 0.02	0.73 ± 0.03
134.9453	-0.0056	0.0527	0.7735	-21.70	8.45 ± 0.07	0.88 ± 0.01	1.45 ± 0.02

Table A2. Same as table A1 but for the Bulgeless class galaxies.

α (J2000)	δ (J2000)	z	$g - r$	$M_{r,\text{tot}}$	$r_{e,d}$	$r_{e,b}$	η_b
212.3728	0.1437	0.0541	0.7417	-20.02	3.59 ± 0.03	-	-
15.7648	13.4973	0.0578	0.7104	-20.12	3.35 ± 0.02	-	-
256.8101	65.3668	0.0537	0.7276	-20.58	3.20 ± 0.02	-	-
121.1723	45.7877	0.0504	0.7333	-20.82	3.66 ± 0.02	-	-
129.1653	47.2543	0.0528	0.8464	-19.72	3.27 ± 0.03	-	-
334.8222	-1.1872	0.0571	0.7529	-19.88	2.58 ± 0.03	-	-
52.5906	0.2631	0.0373	1.1631	-20.34	4.14 ± 0.02	-	-
7.5758	-0.5022	0.0585	0.7055	-20.64	6.32 ± 0.07	-	-
233.1491	49.3842	0.0521	0.7849	-19.89	2.89 ± 0.02	-	-
257.1751	28.5217	0.0451	0.7109	-20.92	4.61 ± 0.01	-	-
209.7411	58.2354	0.0593	0.7557	-20.96	2.33 ± 0.01	-	-
242.0544	44.1528	0.0492	0.7436	-20.15	4.79 ± 0.04	-	-
134.1697	5.8765	0.0592	0.7580	-17.81	3.93 ± 0.05	-	-
145.5350	9.7321	0.0589	0.7888	-19.88	3.26 ± 0.02	-	-
127.3326	6.2958	0.0484	0.7508	-20.92	2.97 ± 0.01	-	-
158.5929	44.3970	0.0522	0.7227	-20.36	2.09 ± 0.01	-	-
204.2524	43.4256	0.0436	0.7958	-20.42	7.24 ± 0.05	-	-
166.6466	44.0469	0.0366	0.7460	-20.04	2.25 ± 0.01	-	-
197.1282	50.6423	0.0293	0.7530	-20.46	2.13 ± 0.00	-	-
199.2471	7.7240	0.0487	0.7647	-20.26	4.07 ± 0.03	-	-
196.6814	9.6532	0.0565	0.7108	-20.42	2.29 ± 0.01	-	-
204.0016	6.5261	0.0231	0.7221	-20.01	2.80 ± 0.01	-	-
243.0000	30.0477	0.0482	0.7935	-20.50	5.30 ± 0.04	-	-
111.0129	40.8093	0.0497	0.9650	-20.06	4.39 ± 0.06	-	-
181.4486	33.8394	0.0539	0.7074	-20.35	3.74 ± 0.05	-	-
249.7326	13.3908	0.0507	0.7658	-20.41	3.83 ± 0.03	-	-
147.9439	27.5461	0.0330	0.7502	-20.52	2.24 ± 0.01	-	-
193.9952	30.3637	0.0512	0.7330	-20.77	4.28 ± 0.02	-	-
159.7373	25.7561	0.0510	1.1405	-20.12	4.81 ± 0.06	-	-
179.4989	25.1587	0.0580	0.7424	-19.97	2.00 ± 0.01	-	-
120.5747	11.4264	0.0600	0.8377	-19.32	2.00 ± 0.01	-	-
153.5945	18.4474	0.0441	0.8836	-19.58	2.17 ± 0.01	-	-
148.8226	17.6874	0.0447	0.8021	-20.43	2.47 ± 0.01	-	-
159.9893	17.6721	0.0571	0.6974	-20.30	4.05 ± 0.04	-	-
171.8496	19.6471	0.0520	0.7675	-19.93	2.22 ± 0.01	-	-
211.4471	15.1940	0.0595	0.7129	-20.72	3.17 ± 0.03	-	-
244.2731	11.4185	0.0402	0.7123	-20.63	3.46 ± 0.01	-	-
165.8052	7.7149	0.0554	0.7294	-20.93	3.35 ± 0.02	-	-

Table A3. Same as tableA1 but for the Bulgy class galaxies.

α (J2000)	δ (J2000)	z	$g - r$	$M_{r,tot}$	$r_{e,d}$	$r_{e,b}$	η_b
55.9895	0.4378	0.0400	0.7490	-21.17	-	4.16 ± 0.07	5.22 ± 0.06
57.6747	1.0408	0.0371	0.7447	-21.13	-	3.62 ± 0.07	5.56 ± 0.06
241.4743	-0.5504	0.0560	0.7526	-21.09	-	3.35 ± 0.08	5.05 ± 0.08
241.2225	-0.0475	0.0520	0.7514	-20.86	-	2.69 ± 0.06	4.80 ± 0.09
243.0857	0.8049	0.0578	0.7354	-21.49	-	6.99 ± 0.35	6.16 ± 0.15
191.5058	-1.0732	0.0474	0.7499	-20.89	-	3.64 ± 0.11	5.56 ± 0.11
239.8879	-1.0989	0.0553	0.7294	-20.92	-	2.72 ± 0.05	3.68 ± 0.06
211.4747	-0.7454	0.0593	0.7498	-21.78	-	4.44 ± 0.08	5.07 ± 0.07
226.1841	-0.3520	0.0548	0.7363	-21.98	-	7.30 ± 0.14	4.83 ± 0.05
244.4877	-0.3815	0.0572	0.7142	-21.14	-	4.05 ± 0.16	6.41 ± 0.14
172.0247	0.1322	0.0495	0.7483	-20.25	-	1.75 ± 0.02	3.34 ± 0.07
217.4984	0.2003	0.0554	0.7196	-20.82	-	2.20 ± 0.05	4.81 ± 0.10
223.4544	0.0897	0.0439	0.7667	-21.20	-	3.60 ± 0.09	6.52 ± 0.09
239.1147	0.0593	0.0397	0.7437	-20.39	-	4.58 ± 0.18	5.92 ± 0.12
247.5797	0.1850	0.0582	0.7267	-20.79	-	3.29 ± 0.11	5.11 ± 0.13
172.6222	0.4943	0.0290	0.7576	-21.10	-	6.26 ± 0.16	5.62 ± 0.07
204.2834	0.4521	0.0479	0.7558	-21.19	-	3.83 ± 0.07	5.22 ± 0.06
222.5090	0.5788	0.0404	0.7378	-21.59	-	4.99 ± 0.14	7.84 ± 0.10
182.7670	0.9723	0.0204	0.7531	-22.33	-	22.11 ± 0.47	6.10 ± 0.04
153.4382	-0.8772	0.0418	0.7437	-20.12	-	4.67 ± 0.23	5.36 ± 0.14
242.5503	0.7837	0.0433	0.7659	-22.17	-	7.77 ± 0.17	5.48 ± 0.09
210.9270	-1.1373	0.0269	0.7541	-20.34	-	2.75 ± 0.03	4.50 ± 0.11
213.7526	-0.7970	0.0385	0.7543	-22.15	-	5.01 ± 0.03	3.98 ± 0.02
214.3278	0.0946	0.0526	0.7821	-21.80	-	8.51 ± 0.22	5.32 ± 0.29
222.7663	-0.4622	0.0432	0.7669	-21.28	-	5.32 ± 0.08	4.11 ± 0.31
193.8191	0.2469	0.0476	0.7537	-22.63	-	9.18 ± 0.13	5.83 ± 0.09

Table A4. Same as table A1 but for the Intermediate- η bulge class galaxies.

α (J2000)	δ (J2000)	z	$g - r$	$M_{r,tot}$	$r_{e,d}$	$r_{e,b}$	η_b
211.8419	-1.0964	0.0551	0.7439	-21.43	7.82 ± 0.06	0.76 ± 0.02	1.52 ± 0.12
227.7024	-1.0625	0.0542	0.7742	-21.64	8.23 ± 0.10	1.17 ± 0.01	1.51 ± 0.02
223.0669	-0.2936	0.0434	0.7345	-21.76	7.09 ± 0.10	2.61 ± 0.12	3.26 ± 0.07
173.8470	0.0906	0.0292	0.6973	-20.31	6.47 ± 0.22	1.31 ± 0.04	3.16 ± 0.06
200.4663	0.1394	0.0347	0.7524	-21.21	5.78 ± 0.03	0.89 ± 0.02	2.89 ± 0.04
211.0308	0.1440	0.0477	0.7341	-21.30	5.50 ± 0.03	0.54 ± 0.02	3.48 ± 0.50
226.1676	0.6045	0.0402	0.7644	-21.56	7.67 ± 0.05	0.93 ± 0.01	1.58 ± 0.02
169.8617	0.9681	0.0399	0.7654	-21.13	4.58 ± 0.04	0.58 ± 0.01	1.66 ± 0.04
190.7771	-0.4379	0.0473	0.8125	-22.33	8.94 ± 0.07	1.62 ± 0.05	2.27 ± 0.06
167.1651	0.2843	0.0249	0.7578	-20.37	3.66 ± 0.02	0.72 ± 0.01	2.56 ± 0.03
189.7547	0.3656	0.0230	0.7874	-21.95	9.02 ± 0.06	1.50 ± 0.01	2.49 ± 0.01
163.6087	0.6637	0.0374	0.7811	-21.24	6.78 ± 0.07	1.12 ± 0.02	2.75 ± 0.05
21.8550	14.0545	0.0236	0.7966	-20.60	5.18 ± 0.10	1.22 ± 0.03	2.40 ± 0.04